

# Momentum distributions of $\alpha$ -particles from decaying low-lying $^{12}\text{C}$ -resonances

R. Álvarez-Rodríguez<sup>1</sup>, A.S. Jensen<sup>1</sup>, E. Garrido<sup>2</sup>, D.V. Fedorov<sup>1</sup>, H.O.U. Fynbo<sup>1</sup>

<sup>1</sup> *Department of Physics and Astronomy, University of Aarhus,  
DK-8000 Aarhus C, Denmark and*

<sup>2</sup> *Instituto de Estructura de la Materia,  
Consejo Superior de Investigaciones Científicas,  
Serrano 123, E-28006 Madrid, Spain*

(Dated: November 18, 2021)

The complex scaled hyperspherical adiabatic expansion method is used to compute momentum and energy distributions of the three  $\alpha$ -particles emerging from the decay of low-lying  $^{12}\text{C}$ -resonances. The large distance continuum properties of the wave functions are crucial and must be accurately calculated. We discuss separately decays of natural parity states: two  $0^+$ , one  $1^-$ , three  $2^+$ , one  $3^-$ , two  $4^+$ , one  $6^+$ , and one of each of unnatural parity,  $1^+$ ,  $2^-$ ,  $3^+$ ,  $4^-$ . The lowest natural parity state of each  $J^\pi$  decays predominantly sequentially via the  $^8\text{Be}$  ground state whereas other states including unnatural parity states predominantly decay directly to the continuum. We present Dalitz plots and systematic detailed momentum correlations of the emerging  $\alpha$ -particles.

PACS numbers: PACS: 21.45.-v; 21.60.Gx; 25.70.Ef; 27.20.+n.

## I. INTRODUCTION

The low-lying resonance states of  $^{12}\text{C}$  have been studied over many years both theoretically and experimentally, motivated partly by their astrophysical importance [1, 2, 3, 4, 5, 6, 7, 8, 9, 10]. Surprisingly, many issues are still not really understood, e.g. the energies, angular momenta, structure and decay properties of the resonances. Completely open questions still remain on the  $2^+$  resonances. Morinaga conjectured in the fifties that a  $2^+$  state should exist around 9 MeV as a member of the rotational band with the  $0^+$  resonance at 7.65 MeV as band-head [1]. Several experiments recently provided new results [11, 12, 13] but unfortunately no agreement has yet been reached for the position and width of the first  $2^+$  resonance.

Attempts to obtain information about the spectrum from decay measurements immediately face the problem that only the final state is observed. Properties of the initial state must then be reconstructed from the momentum distributions of the three fragments after the decay. Both initial state and the intermediate paths connecting initial and final states are not observables. These configurations can therefore only be described through model interpretations. This is somewhat different in reaction experiments, where information can in addition be extracted from properties of outgoing particles in transfer or scattering reaction.

If we assume that the initial state is a resonance populated one way or another, and that its decay is independent of the previous history. This is a simplification decoupling the formation from the decay in analogy to compound nuclear reactions. The decay process can then be viewed as a stationary wave function connecting initial and final states through a continuous series of intermediate configurations. This is equivalent to a time dependent process where the initial state, formed at small distances, evolves through the intermediate configurations and re-

sults in the final state at large distances. This implies a steady state outgoing flux described precisely by the stationary resonance wave function.

Thus the resonance wave function can be interpreted as reflecting the decay mechanisms. Two principally different modes are traditionally considered, i.e. sequential decay via an intermediate two-body configuration, and decay directly into the three-body continuum. In both cases the final state is embedded in the three-body continuum and the modes can only be distinguished if the momentum distributions carry unique information characterizing one of the modes. Otherwise the distinction becomes fluent or a matter of an artificial, although perhaps more precise, model definition. Previous approaches to describe this type of observables have been performed mainly for the  $1^+$  states, e.g. Faddeev calculations [14], R-matrix computations, which describe their decay as sequential [15], and Kurchatov fitting, which describes them as direct or democratic [16].

The purpose of this paper is to present  $\alpha$ -particle momentum distributions and Dalitz plots [17] after decays of all the computed  $^{12}\text{C}$ -resonances [18] below the proton separation threshold at an excitation energy of 15.96 MeV, where only  $3\alpha$ -decay is possible. These distributions should help to establish spins and parities of the yet unknown levels. They provide then information about structures of initial and intermediate states. Combined with the measurements a more complete picture of the  $^{12}\text{C}$ -spectrum and the decay mechanisms should then emerge. In section 2 we first sketch the theoretical framework and the choice of interactions. The results are presented and discussed in section 3 for both unnatural and natural parity states. Section 4 contains a summary and the conclusions.

## II. THEORETICAL FRAMEWORK

The resonances decay into three particles, therefore we need a theoretical tool to describe this three-body continuum structure. We employ the hyperspherical complex rotated [19, 20] adiabatic expansion [21] in coordinate space to compute bound states and resonances. This method is able to deal with several simultaneously bound and nearly bound two-body states in different subsystems. Relatively large distances can often be calculated accurately with a specific choice of basis and partial waves. The Fourier transform of the wave function provides the observable momentum distributions. The three-body model consisting of  $\alpha$ -particles requires interactions which reproduce energies and scattering properties of the  $\alpha$ - $\alpha$  system.

### A. Practical procedure

We describe  $^{12}\text{C}$  as a  $3\alpha$ -cluster system at all distances. We use Faddeev equations and solve them in coordinate space using the adiabatic hyperspherical expansion method [20, 21, 22]. The hyperspherical coordinates consist of the hyperradius  $\rho$  and five generalized angles. The angular Faddeev decomposed wave functions,  $\Phi_{nJM} = \sum_{i=1}^3 \Phi_{nJM}^{(i)}$ , are chosen for each  $\rho$  as the eigenfunctions of the angular part of the complex scaled ( $\vec{r} \rightarrow \vec{r} \exp(i\theta)$ ) Faddeev equations

$$(T_\Omega - \lambda_n) \Phi_{nJM}^{(i)} + \frac{2m}{\hbar^2} \rho^2 V_i \Phi_{nJM} = 0 \quad i = 1, 2, 3. \quad (1)$$

$T_\Omega$  is the angular part of the kinetic energy operator and  $V_i$  is the potential between particles  $j$  and  $k$ , being  $\{i, j, k\}$  a cyclic permutation of  $\{1, 2, 3\}$ . The total wave function,  $\Psi^{JM}$ , is expanded on the hyper-angular eigenfunctions, i.e.

$$\Psi^{JM} = \frac{1}{\rho^{5/2}} \sum_n f_n(\rho) \Phi_{nJM}(\rho, \Omega), \quad (2)$$

where the  $\rho$ -dependent expansion coefficients,  $f_n(\rho)$ , are the hyperradial wave functions obtained from the coupled set of hyperradial equations

$$\begin{aligned} & \left( -\frac{\partial^2}{\partial \rho^2} + \frac{15/4}{\rho^2} + \frac{2m}{\hbar^2} [W_n(\rho) + V_{3b}(\rho) - E] \right) f_n(\rho) \\ & = \sum_{n'=1}^{\infty} \hat{P}_{nn'} f_{n'}(\rho) \end{aligned} \quad (3)$$

$W_n(\rho)$  are the angular eigenvalues of the three-body system Hamiltonian with fixed  $\rho$ ,  $V_{3b}$  is the three-body potential,  $E$  is the three-body energy and  $\hat{P}_{nn'}$  are the non adiabatic terms. The eigenvalues  $W_n(\rho)$  of the angular equations eq. (1) serve as effective potentials.

In order to obtain the resonances we use the complex scaling method. According to this method, the energy

and width of a resonance state are associated with the complex eigenvalues of a certain analytically continued Hamiltonian operator. The appropriate operator results from the rotation of the position vectors of the ordinary Hamiltonian into the complex coordinate plane

$$\vec{r} \rightarrow \vec{r} e^{i\theta} \quad \theta > 0, \text{ real}. \quad (4)$$

This gives rise to the complex-rotated Hamiltonian

$$H_\theta(\vec{r}) = H(\vec{r} e^{i\theta}). \quad (5)$$

The complex energy of a resonance corresponds to a pole in the momentum-space wave function, while in coordinate-space this form corresponds to a large-distance asymptotic wave function consisting of outgoing waves. In other words, the three-body resonance corresponds to a complex energy solution  $E_0 = E_R - i E_I$  of the system (3) with the asymptotic boundary condition of an outgoing wave in every channel  $n$

$$f_n(\rho \rightarrow \infty) = C_n e^{+i \kappa \rho}, \quad (6)$$

where  $C_n$  is an asymptotic normalization coefficient and  $\kappa = \sqrt{2mE/\hbar^2}$  is the three-body momentum or the conjugate of  $\rho$ . It has been seen that this boundary condition determines that the scattering matrix has a pole at the complex energy  $E_0$ , being  $E_R$  the position of the resonance and  $\Gamma = 2E_I$  its width.

The  $^{12}\text{C}$ -resonances are not necessarily of three-body character even though this by definition must be the case at large distances for  $3\alpha$ -decay. We use the three-body model also at small distances because, like in Gamow's theory of  $\alpha$ -decay, the detailed structure at small distances is not important for the decay properties which only require the proper description of the emerging three particles. We use the three-body short-range potential to adjust the corresponding small-distance part of the effective potential to reproduce the correct resonance energies which are all-decisive for decay properties as evident in the probability for tunneling through a barrier.

At intermediate distances the three  $\alpha$ -particles are formed and the potential has a barrier that determines the partial width of the resonance. At large distances the resonance wave functions contain information about distributions of relative energies between the three particles after the decay. These properties are connected to the many-body properties at small distances via preformation factors, as in  $\alpha$ -decay. An adjustment of the resonance energy is then needed. After complex rotation the resonance wave function is characterized by an exponential fall-off at large distance. Thus the crucial information is found in relative sizes of the very small values,  $f_n$ , of the resonance at large distances which are very difficult to compute accurately especially when the Coulomb interaction is present.

## B. Momentum distributions

The complex scaled coordinate space resonance wave function should be rotated back to real coordinates and Fourier transformed to provide the observable momentum distributions. Unfortunately the corresponding integral is not convergent and a regularization procedure has to be applied. The origin is simply that the resulting wave function should be a non-normalizable outgoing plane wave at large distances. We overcome this problem with the Zeldovic regularization procedure which is well defined for short-range interactions [20]. In total this amounts to using the angular part of the coordinate space wave function at a large hyperradius, but interpreted as the momentum space wave function. Inclusion of the Coulomb interaction is achieved by treating it as an ordinary potential up to a large value of the hyperradius and then extrapolate the diagonal parts of the adiabatic wave functions with the numerically obtained Coulomb and centrifugal potentials.

Two different cases must be treated, i.e. sequential and direct decays distinguished theoretically by the structure of the adiabatic wave functions [23]. Direct decay is characterized by structures where all particles are far apart and as the hyperradius increases all distances increase proportionally. The Zeldovic regularized Fourier transform of the resonance wave function gives in this case the momentum distributions [24].

Sequential decay is characterized by a wave function describing a bound-state like structure of two close-lying particles supplemented by the third particle far away. For a complex scaled wave function such a structure would be that of a two-body resonance, provided the rotation angle  $\theta$  is larger than the angle corresponding to the energy and width of this resonance. These structures approach two-body bound state configurations as the hyperradius increases.

However, Fourier transformed and rotated back to the real axis, the wave function should at large distances approach the description of the third particle (plane or Coulomb wave) leaving the decaying resonance which has the given two-body energy and width. This is two sequential two-body decays, hence the characterizing notation. The resulting momentum distributions cannot be obtained from the rotated wave function but should instead be calculated from the correct physical description of two two-body decays. This results in a Breit-Wigner distribution for the third particle with a width equal to the sum of two-body and initial three-body resonance widths peaking around the energy found by subtracting the two-body from the three-body energies.

## C. Interactions

The basic ingredients are the two-body interactions,  $V_i$ , between particles  $j$  and  $k$ , where  $\{i, j, k\}$  is a cyclic permutation of  $\{1, 2, 3\}$ . First  $V_i$  must reproduce the low-

energy two-body scattering properties which can be obtained independently for each partial wave resulting in angular momentum dependent or non-local interactions. We rely on the experience gained previously especially through [18], and we choose an Ali-Bodmer potential [25] slightly modified in order to reproduce the s-wave resonance of  ${}^8\text{Be}$ . The phase shifts are essentially unchanged and reproduce  $\alpha - \alpha$  scattering data but in order to describe sequential decays properly the two-body subsystems must also have the correct energies. In total we use a potential given as

$$V_{\alpha\alpha} = \left(125\hat{P}_{l=0} + 20\hat{P}_{l=2}\right) e^{-r^2/1.53^2} - 30.18e^{-r^2/2.85^2}, \quad (7)$$

where lengths are in fm and strengths are in MeV. The operators  $\hat{P}_l$  project on angular momentum.

The three-body resonance energy and wave function can now be computed but the energy usually does not coincide with the measured value. It may be close, indicating that the three-body structure is nearly correct. Then only fine-tuning is needed due to the neglected smaller three-body effects of polarization or excitations of intrinsic particle degrees of freedom or off-shell effects. We emphasize that only three-body effects are missing since the two-body data already is reproduced by the phenomenological two-body interactions. We then correct the energy by including a diagonal three-body short-range interaction chosen to be Gaussian in hyperradius, i.e.  $V_{3b} = S \exp(-\rho^2/b^2)$ . The structures of the resonances are then maintained [26]. A larger range corresponding to a third order power law is not selected as e.g. in [27] where it is used to compensate for the limitation in Hilbert space due to the hyperharmonic expansion in only one Jacobi coordinate. Our better basis confines the three-body interaction to be genuinely of short-range character.

In the actual parameter choice we prefer to maintain the same values of  $b$  and  $S$  for different states with the same angular momentum and parity  $J^\pi$  but allow variation with  $J^\pi$ . To see the systematic behavior we then decided to fix  $b = 6$  fm corresponding to the hyperradius obtained when the three alphas are touching in an equilateral triangle. The strength  $S$  is then adjusted to reproduce one of the observed resonance energies. The main dependence is indirect through the variation of the three-body energy and much less through the shape of the total potential [18]. In this way we attempt to separate the effects of the initial many-body structure from the symmetries related to the angular momentum conservation. The strongest influence is expected from Coulomb potentials and centrifugal barriers.

## III. COMPUTED DISTRIBUTIONS

We find  ${}^{12}\text{C}$ -resonances below 15.96 MeV for most angular momenta  $J \leq 6$  and all parities, i.e. two  $0^+$ , three

$2^+$ , two  $4^+$ , and one of each of  $1^\pm$ ,  $2^-$ ,  $3^\pm$ ,  $4^-$  and  $6^+$  [18]. Their structures were described in detail in [18] including the variation with possible interaction parameters. However, only small and intermediate distance properties are important for energies, widths and partial wave decomposition. The final state momentum distributions after decay arise from the large distance properties which are much more difficult to determine numerically.

The procedure is to compute ratios of radial wave functions at large distances. This supplies the relative weights on the contributions from each of the adiabatic wave functions. First we have to remove the contributions from the wave functions corresponding to population of two-body resonances. These fractions must be computed as consecutive two-body decays and their contributions added to the remaining results from direct decays which are found by absolute square of the wave function at a large hyperradius followed by integration over the unobserved angular variables.

The asymptotic large-distance behavior should be reached by increasing the partial waves and the basis size used. This convergence can be tested by showing independence of the results with variation of the largest value of the hyperradius. Failing the test implies that the basis size is too small, or contrarily a larger hyperradius can be compensated by a larger basis producing the same result. It is then economical to get stability for a hyperradius and basis as small as possible. In most cases we find that the asymptotic behavior is reached for hyperradii larger than about 60 fm. There is a small variation of the distributions from 70 to 100 fm, and we have chosen 80 fm as the value of  $\rho$  where the energy distributions are computed.

The results fall in two groups of natural and unnatural parity states, e.g. implying that sequential decay through  ${}^8\text{Be}(0^+)$  is either allowed or forbidden by conservation of angular momentum and parity. Decay through  ${}^8\text{Be}(2^+)$  is possible in both cases but this state is rather broad and the result would be hard to distinguish from direct decay. We see no indication of population of this channel in the numerical results. To optimize the accuracy we then maintain as small a scaling angle as possible consistent with distinct separation of the three-body resonance from the background continuum.

### A. Unnatural parity states

These states are  $1^+$ ,  $2^-$ ,  $4^-$  and  $3^+$  and our basis describes them as decaying directly although analyses of measured distributions employ interpretations as sequential through  ${}^8\text{Be}(2^+)$  [13, 28, 29].

The lowest  $1^+$  state was briefly discussed previously in [23, 30]. Experimentally two  $1^+$  states, isospin 0 and 1, are known but we find only one reflecting that we are confined to isospin 0 by using  $\alpha$ -particles as building blocks. Both states are very far from resembling  $\alpha$ -cluster states. Still the decays of both states must proceed through the

same  $\alpha$ -cluster configurations, although the weights on the adiabatic potentials might differ from state to state. Underlying many-body effects are beyond the present model but we can pinpoint the neglected effects, i.e. the preformation factors established at small distances where the many-body problem is constraint into a three-body problem, and better three-body potential to account for the transition between the  $N$ - and three-body degrees of freedom at short and large distances, respectively. For these reasons the contributions from the individual adiabatic potentials could differ for decays of these two  $1^+$  states of different isospin.

We first focus on the isospin 1 state at an excitation energy of 14.98 MeV (7.70 MeV above threshold). We adjust the three-body potential and compute the energy distributions shown in Fig.1. The upper part exhibits the Dalitz plot and the lower part projects the distribution on the axis with one  $\alpha$ -particle energy. The latter is computed by using Monte Carlo integration over all phase space directly from the wave function.

The measured distributions [31] are very uncertain first of all because the lower-lying isospin zero  $1^+$  state at 12.70 MeV (5.42 MeV above threshold) also is populated via feeding from a gamma transition between the two  $1^+$  states. This contribution is not easily removed from the existing data to allow a clean comparison. A better analysis or a new experiment measuring the  $\alpha$ -decay of the  $T=1$   $1^+$  state in complete kinematics is required. Our computed result is almost identical to the distributions, measured and calculated, for the 12.70 MeV state [23, 29] if the difference in available energy is corrected for. The distributions in Fig.1 are then direct prediction based on the assumptions that the isospin zero components in both states are equally populated and decay through the same mechanism.

A test of this prediction would provide interesting information about the dynamics of isospin mixing. Two extremes can be imagined, i.e. the same isospin 0 components can be present from small to large distance resulting in the same distribution, or different complicated many-body structures at small distances clusterize into  $\alpha$ -particles around the nuclear surface and proceed to detection at large distances. We know that the partial decay widths for both states are much smaller than predicted from the cluster model [18] but this information does not prohibit the momentum distributions from being almost identical.

In the computation we find only one of each state of even  $J$  and negative parity, i.e. one  $2^-$  one  $4^-$  state. The experimental spectrum has two states of  $2^-$  where the highest at 13.26 MeV (5.98 MeV above threshold) only is tentatively assigned to have  $2^-$  [32] while no  $4^-$  state is found experimentally. It is then tempting to believe that this state at 13.26 MeV really is a  $4^-$  state as indicated by our computations [33]. This new spin-parity assignment has also been suggested recently in [34].

One way to decide which spin and parity is correct is to measure the momentum distributions of the fragments

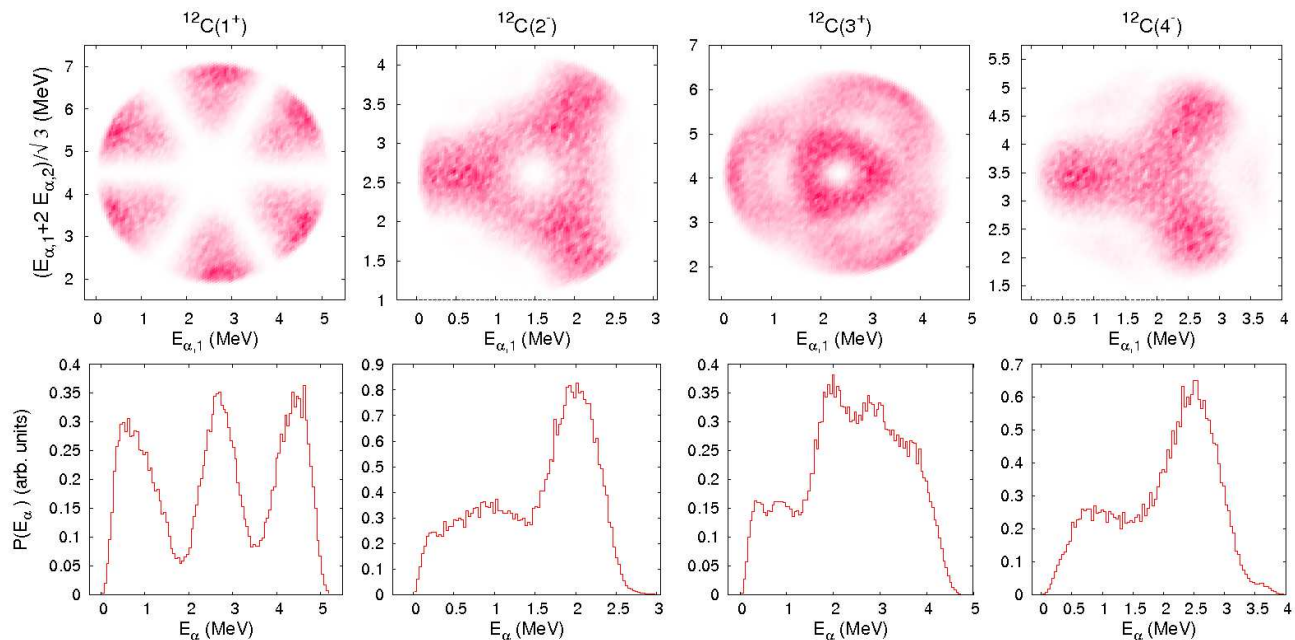


FIG. 1: Dalitz plot (upper part) and the  $\alpha$ -particle energy distribution (lower part) for the  $(1^+, 2^-, 3^+, 4^-)$ -resonances at an excitation energy of (14.98, 11.80, 14.40, 13.26) MeV or (7.70, 4.53, 7.13, 5.98) MeV above the  $3\alpha$  threshold, which is 7.275 MeV above the ground state. We have performed a Monte Carlo integration over the phase space, which due to the statistical nature produces the unphysical fluctuations.

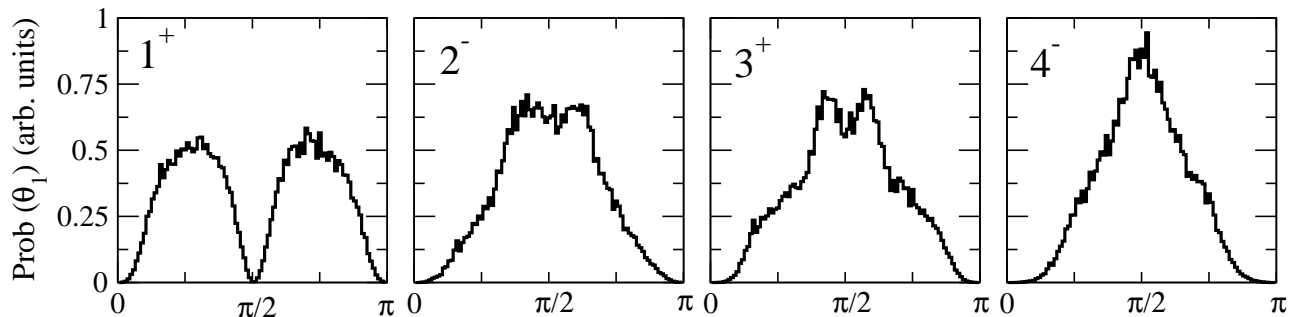


FIG. 2: The angular distributions of the directions between two particles and their center of mass and the third particle for the  $(1^+, 2^-, 3^+, 4^-)$ -resonances in Fig.1. We have performed a Monte Carlo integration over the phase space, which due to the statistical nature produces the unphysical fluctuations.

emerging after decay. Usually this carries distinct signatures of the angular momentum of the decaying state. In [35, 36] it is shown that, even within non-sophisticated theoretical models, the basic signatures of the angular momentum are present in the experimental data. We first turn to the energy distributions in Fig.1. Both  $2^-$  and  $4^-$  show very similar distributions but the peaks appear at slightly higher values for the  $4^-$  state. However, the two-dimensional Dalitz plots differ more from each

other. Both have the triangular symmetry but the  $2^-$  resonance have virtually nothing in between these peaks in contrast to the somewhat more smeared out distributions of the  $4^-$  resonance.

In the computations we find also a  $3^+$  resonance for which there is no experimental evidence, but it has been suggested in [34] to assign these quantum numbers to the state at about an excitation energy of 13.35 MeV. Theoretically a  $3^+$  state has also been found in [4]. With

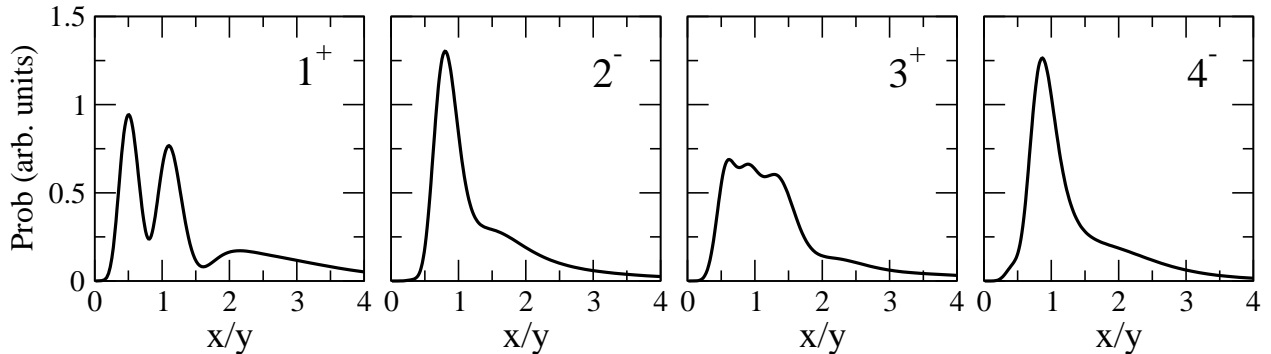


FIG. 3: The distributions of the ratio of the distances between two particles and their center of mass and the third particle for the  $(1^+, 2^-, 3^+, 4^-)$ -resonances in Fig.1.

a reasonable three-body strength, -20 MeV, placing the state at 14.40 MeV (7.13 MeV above threshold), we find the energy distributions in fig. 1. The distribution is very broad but peaked at intermediate energies. This is seen to arise from a Dalitz plot distribution with a small hole in the middle surrounded by a close-lying dense circle and a much larger diffuse distribution.

The angular momentum may leave an even more distinct signature in the angular distributions, shown in Fig.2, of the directions between two particles and their center of mass and the third particle. The information is then directly about the corresponding angular momentum denoted as  $\ell_y$ , i.e. the angular momentum of the third particle relative to the center of mass of the other two with the relative angular momentum  $\ell_x$ . We see that the angular distribution patterns are quite different for different states. The  $1^+$  distribution shows two broad peaks separated by a minimum with vanishing probability at an angle of  $\pi/2$ .

This reflects that the partial wave components in the angular wave function are a linear combination of only  $(\ell_x, \ell_y) = (2, 2), (4, 4)$  each coupled to the resulting value of 1 [23]. Choosing the specific directional angles of  $\phi_x = \phi_y = \theta_x = 0$  and  $\theta_y = \pi/2$  we find that only projection quantum numbers of  $m_x = 0$  and  $m_y = 0, \pm 2, \pm 4$  give non-vanishing contributions. This is only consistent with a projection of the total angular momentum  $M = m_x + m_y$  since  $M = m_y = \pm 1$  gives zero. However when all projections are zero the Clebsch-Gordan coupling coefficient is also zero. The observables in Fig.2 reveal information about the intrinsic angular momenta used to construct the wave function.

In contrast both  $2^-, 3^+$  and  $4^-$  have peaks in the distributions at  $\pi/2$ . The different shapes can be traced back to the different partial wave decomposition computed and discussed in [23], i.e.  $2^-$  has about 40% to 60% of  $\ell_y = 1, 3$ , while  $4^-$  is dominated by  $\ell_y = 3$ , and  $3^+$  has about twice as much  $\ell_y = 2$  as  $\ell_y = 4$ . These features are clearly distinguishable demonstrating that these observables can be used to determine the large-distance structure of these resonances. The initial state can still

only be determined through the theoretical information about the dynamical evolution of the resonances.

The one-dimensional distributions in Fig.1 can be used to extract the distributions of how far the three particles are from each other [37]. This is visualized by a triangle with a particle in each corner moving apart from their common center of mass. In particular the distributions of the ratio,  $x/y$ , of the distances between two particles,  $x$ , and their center of mass and the third particle,  $y$ , are shown in Fig.3. Since all Jacobi systems are identical we do not have to distinguish between Jacobi sets. Unfortunately the symmetric wave function then do not allow distinction between these identical particles.

With several peaks as for the  $1^+$  resonance the interpretation is obvious, namely that each peak contains one  $\alpha$ -particle. The triangular geometric structure for the decay of this isospin one  $1^+$  state then corresponds to side ratios of 2.2:1.8:1 of the triangle. For the other unnatural parity states only one broad peak is seen close to the value 1. For an equilateral triangle the  $x/y$ -ratio is  $2/\sqrt{3} \approx 1.15$  which then is the only value where a narrow peak is possible. Otherwise a broader peak must cover overlapping distributions deviating somewhat from the equilateral triangle and corresponding to similar but less symmetric configurations.

## B. Natural parity states

These states are  $0^+, 1^-, 2^+, 3^-, 4^+$  and  $6^+$ . They can decay via the energetically favorable  ${}^8\text{Be}(0^+)$  which asymptotically must be described by one of the adiabatic potentials with the  ${}^8\text{Be}+\alpha$  structure. The signature is simply that this potential approaches the complex energy of the  ${}^8\text{Be}(0^+)$  resonance. The radial resonance wave functions at large distances determine the population fractions for each of the adiabatic potentials. In particular we can find the fraction of decay proceeding sequentially through this  $0^+$ -state, and furthermore we can compute the related distributions as two consecutive

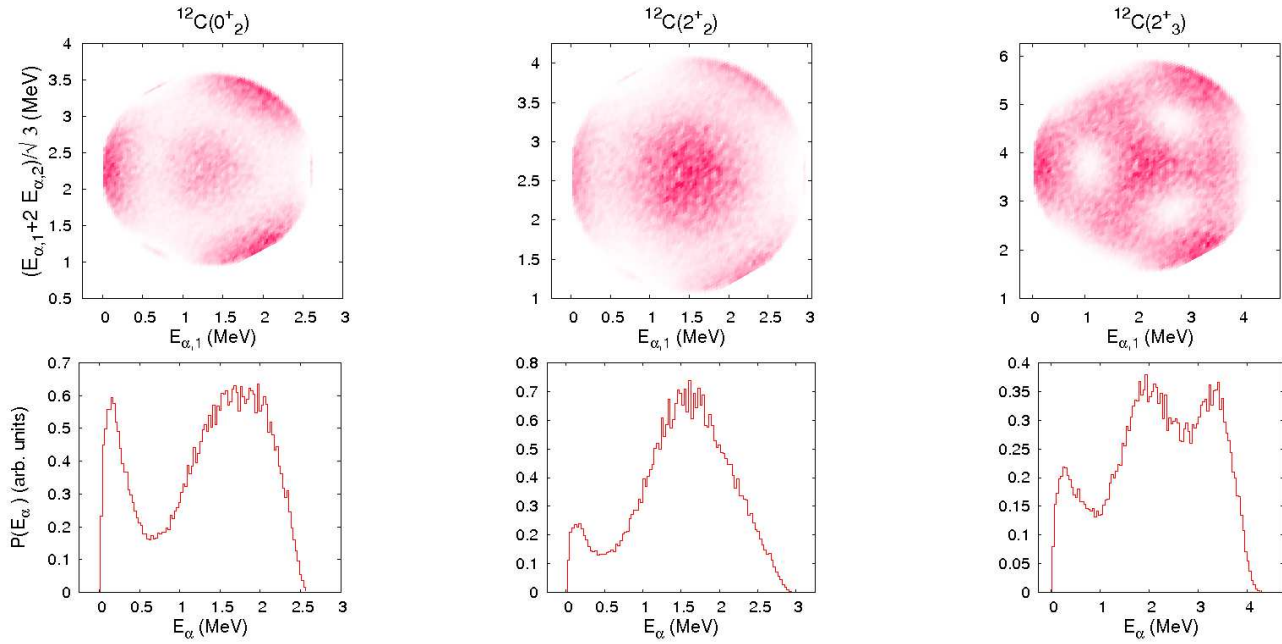


FIG. 4: Dalitz plot (upper part) and the  $\alpha$ -particle energy distribution (lower part) for the  $(0_2^+, 2_2^+, 2_3^+)$ -resonances at an excitation energy of (11.22, 11.76, 13.76) MeV or (3.95, 4.48, 6.49) MeV above the  $3\alpha$  threshold, which is 7.275 MeV above the ground state. We have performed a Monte Carlo integration over the phase space. The sequential decay, respectively of 59%, 15%, 4%, through  $^8\text{Be}(0^+)$  is removed. We label as in table I.

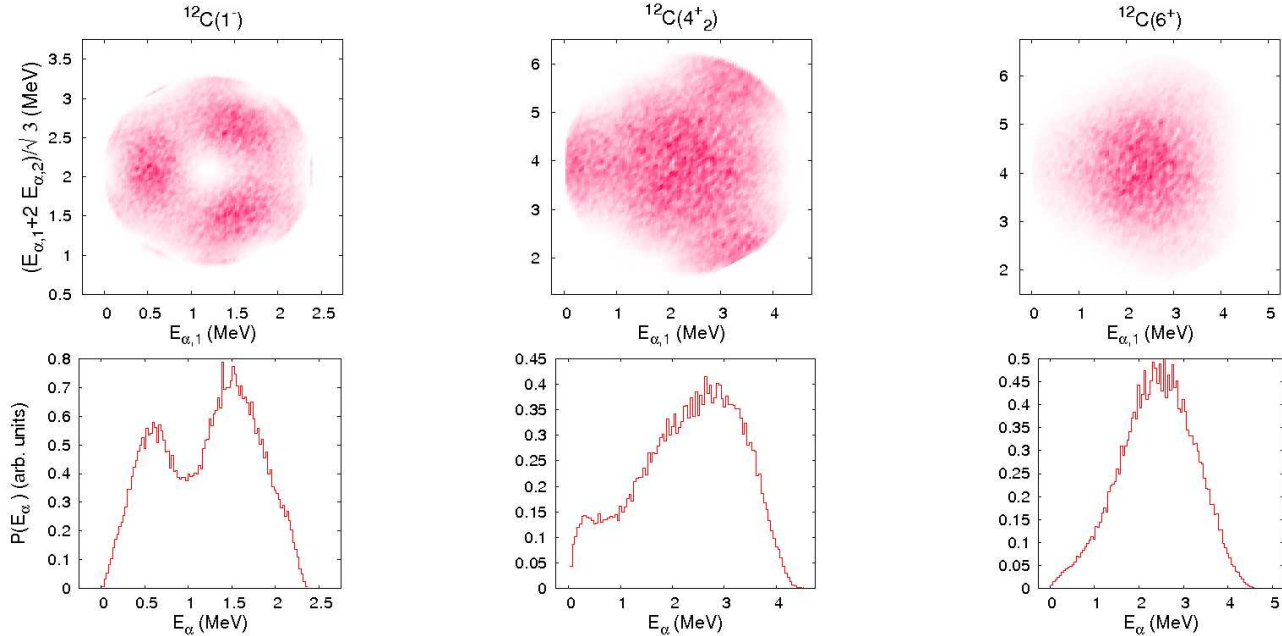


FIG. 5: Dalitz plot (upper part) and the  $\alpha$ -particle energy distribution (lower part) for the  $(1^-, 4_2^+, 6^+)$ -resonances at an excitation energy of (10.88, 14.10, 14.40) MeV or (3.61, 6.83, 7.13) MeV above the  $3\alpha$  threshold, which is 7.275 MeV above the ground state. We have performed a Monte Carlo integration over the phase space. The sequential decay, respectively of 70%, 20%, 5%, through  $^8\text{Be}(0^+)$  is removed. We label as in table I.

TABLE I: Energy above the triple- $\alpha$  threshold, excitation energy and estimated amount of sequential via  ${}^8\text{Be}(0^+)$  and direct decays for the natural parity states of  ${}^{12}\text{C}$ . If necessary we label the resonances with increasing energy above threshold.

$J^\pi$	$E_{\alpha\alpha\alpha}$ (MeV)	$E_{exc}$ (MeV)	sequential	direct
$0_1^+$	0.38	7.66	95%	5%
$2_1^+$	1.38	8.66	97%	3%
$3_1^-$	2.33	9.60	96%	4%
$4_1^+$	3.25	10.52	92%	8%
$1_1^-$	3.61	10.88	70%	30%
$0_2^+$	3.95	11.22	59%	41%
$2_2^+$	4.48	11.76	15%	85%
$2_3^+$	6.49	13.76	4%	96%
$4_2^+$	6.83	14.10	20%	80%
$6^+$	7.13	14.40	5%	95%

two-body decays.

The result is one peak close to an energy of  $E_{max} = 2E_\alpha/3$  with a width roughly equal to the width of the decaying state, and a broader square-like peak at an energy of about  $E_{max}/4$  determined by kinematics. Here we assumed vanishing energy and width of  ${}^8\text{Be}(0^+)$ , otherwise the peak positions and widths should be modified. The Dalitz plots should also reflect these features by showing one high-energy, almost vertical, single- $\alpha$  distribution, and two separated (for each of the other  $\alpha$ -particles) more horizontal distributions corresponding to a broader peak after projection on the single  $\alpha$ -energy  $x$ -axis.

The angular distribution from sequential decay through  ${}^8\text{Be}(0^+)$  must reflect the behavior of the angular momentum  $\ell_y$  precisely as for ordinary decays of a quantum state of given angular momentum. The direct decay is expected to give a relatively broad distribution shifted from the central value at half the maximum energy by an appropriate average over the combinations of angular momentum phase space factors. This can also be interpreted geometrically as an expanding triangular configuration with given side ratios.

First we extract the percentage of sequential decay via  ${}^8\text{Be}(0^+)$  and direct decay for the natural parity states, see table I. The lowest-lying natural parity states of each  $J^\pi$  ( $0^+$ ,  $2^+$ ,  $3^-$  and  $4^+$  states with excitation energies 7.66 MeV, 8.66 MeV, 9.60 MeV and 10.52 MeV) seem to be completely dominated by decays via  ${}^8\text{Be}(0^+)$ . In contrast, the highest-lying  $2^+$  state at 13.76 MeV excitation energy and the  $6^+$  state at 14.40 MeV excitation energy only have small fractions decaying through the  ${}^8\text{Be}$  ground state. In the remaining cases ( $1^-$ ,  $0^+$ ,  $2^+$  and  $4^+$  states with excitation energies 10.88 MeV, 11.22 MeV, 11.76 MeV and 14.10 MeV) both mechanisms are comparable.

The lowest of the two  $0^+$  resonances is the so-called Hoyle state, which plays an important role in nuclear astrophysics. According to our computation, it decays almost entirely sequentially. Very little is left for the direct decay which therefore is not shown. The experimental distribution is also consistent with complete domina-

tion of sequential decay as in our computation [23]. We also omit the other three natural parity resonances dominated by sequential decays. We concentrate instead on the 6 resonances where a substantial amount is direct decay. These distributions are shown in Figs. 4 and 5 after removal of the contributions from the sequential decay through the  ${}^8\text{Be}$  ground state. The experimental analyses can extract the trivial contribution from the decay through the  ${}^8\text{Be}$  ground state. It is therefore straightforward to make a comparison with the experiment. Both Dalitz plots and projected single- $\alpha$  energy distributions are shown.

The higher-lying  $0^+$  resonance has a large width of about 3.5 MeV. On top of this difficulty the population through beta-decay of the corresponding energy region leads to violation of the independent approximation of formation and decay of the resonance. The main effect is a shift in energy of the resonance position. In any case this state has a significant probability of decaying directly into the three body continuum. This part, shown in fig. 4, exhibits a triangular structure in the Dalitz plot, but now we find one low-energy  $\alpha$ -particle and two of moderate energies. This is in almost complete contrast to the sequential decay where one energy is high and two are small.

Next we focus on our results in connection with the existence and position of low-lying  $2^+$  resonances which still is an open question for the  ${}^{12}\text{C}$  nucleus. The old suggestion is that the Hoyle state should be the band-head followed by a  $2^+$  state at around 10 MeV [1]. There are experimental indications for the existence of such a state [29] but no consensus has so far been reached. On the other hand other theoretical models, also cluster models, find three  $2^+$  resonances in this energy region [38]; in [4] two  $2^+$  excited states are found in this region, while in [6] one  $2^+$  state appears below 12.3 MeV excitation energy. We find rather different structures for these three states, still all of  $\alpha$ -cluster structure. Each of them is dominated by its own adiabatic wave function corresponding to three different low-lying adiabatic potentials with differing partial wave decomposition [18]. Most likely these states are hidden behind broad states of roughly the same energy. They are therefore extremely difficult to distinguish from the background in any of the experiments.

Their decay properties also vary substantially, e.g. the percentage of sequential decay through  ${}^8\text{Be}(0^+)$ , see table I. The lowest state almost exclusively decays sequentially while the other two mostly decay directly. In fig. 4 we see that the direct parts give very broad distributions. For the second  $2^+$  resonance all three  $\alpha$ -particles emerge with large probability with similar kinetic energies. For the third  $2^+$  resonance the distribution is more diffuse and the energies are more unevenly divided resulting in a structured but relatively broad distribution.

We continue with the  $1^-$  state, both Dalitz plot and one-dimensional projection are shown in Fig. 5 for the 30% decaying directly into the three-body continuum. A similar triangular structure as for the second  $0^+$  reso-



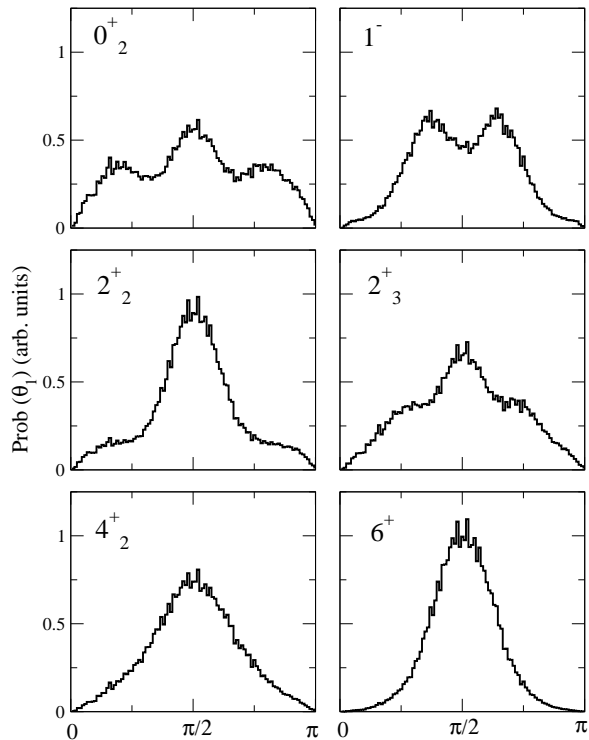


FIG. 6: The angular distributions of the directions between two particles and their center of mass and the third particle for the ( $0_2^+$ ,  $1^-$ ,  $2_2^+$ ,  $2_3^+$ ,  $4_2^+$ ,  $6^+$ )-resonances in Figs.4 and 5. We have performed a Monte Carlo integration over the phase space. The sequential part is removed as in figs. 4 and 5. We label as in table I.

nance is seen although substantially more smeared out resulting in two overlapping broad peaks after projection on the  $x$ -axis.

Both the  $3^-$  resonance and the lowest of the two  $4^+$  resonances are almost completely dominated by sequential decay. The second of the  $4^+$  resonances gives a rather diffuse distribution of kinetic energy of the  $\alpha$ -particles, see fig. 5. It resembles somewhat the distribution from the third  $2^+$  resonance except that the small probability holes in the Dalitz plot now also are smeared out. This distribution is again almost the opposite of the sequential decay distribution with one high and two low energy particles. The  $6^+$  resonance has a symmetric distribution extending about 1 MeV around a central region where all energies are roughly equal.

We now turn to the other type of information found in the angular distributions which exhibit the correlated directions of emergence. Obviously the sequential decay through the  ${}^8\text{Be}(0^+)$  state must be with the third  $\alpha$ -particle in the opposite directions of  ${}^8\text{Be}$ . The only information here is then about the partial wave component ( $\ell_y$ ) of that third particle relative to  ${}^8\text{Be}$ . Angular

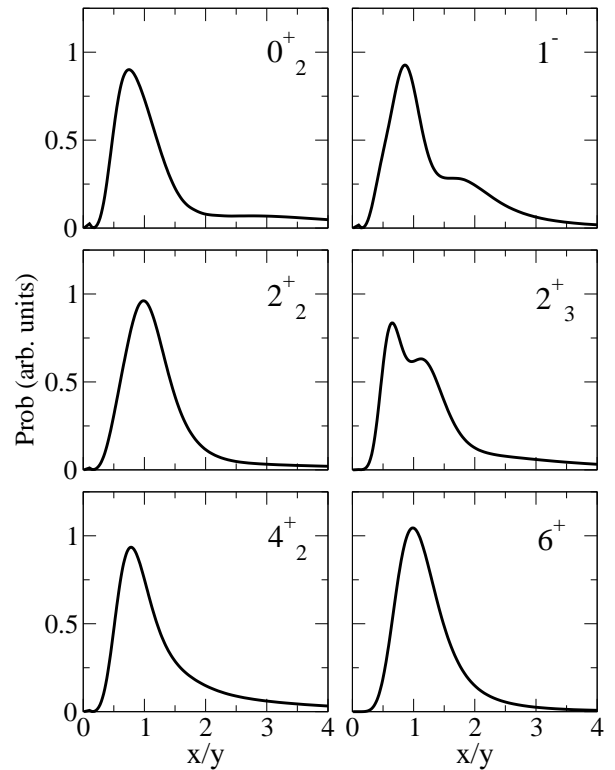


FIG. 7: The distributions of the ratio of the distances between two particles and their center of mass and the third particle for the ( $0_2^+$ ,  $1^-$ ,  $2_2^+$ ,  $2_3^+$ ,  $4_2^+$ ,  $6^+$ )-resonances in Fig.4. The sequential part is removed as in figs. 4 and 5. We label as in table I.

momentum conservation then requires the total angular momentum  $J = \ell_y$ . Thus the most interesting new information is contained in the directly decaying parts shown in Fig.6. These distributions also vary from state to state reflecting the structure in terms of partial waves as discussed in [18].

The distribution corresponding to  $0_2^+$ -state is essentially from the isotropic distribution of  $\ell_y = 0$  modified by a smaller contribution from  $\ell_y = 2$  with maxima at  $\pi/4$  and  $3\pi/4$  separated by zero probability at  $\pi/2$ . The distribution corresponding to  $1^-$  shows two peaks separated by a small minimum at  $\pi/2$ . The largest partial waves are here  $\ell_y = 1, 3$ . The angular distributions of both the second and third  $2^+$  resonance seem to contain a narrow peak on top of a broader one. These structures are due to large contributions from  $\ell_y = 0$  supplemented by contributions from  $\ell_y = 2$  and  $\ell_y = 4$ , respectively. Finally, the distributions form  $4_2^+$  and  $6^+$  both exhibit one smooth, and for  $6^+$  also relatively narrow, peak around  $\pi/2$ . The partial wave structures of these states are mainly  $\ell_y = 2$ , and  $\ell_y = 2, 4$ , respectively

We again attempt to extract the geometric structure of the dominating triangular decay configurations. The

results for the ratio between one pair of particles and their center of mass and the third particle are shown in Fig.7. They are all rather similar with a relatively broad peak around 1, but for  $1^-$  and  $2_3^+$  with more structure at a larger ratio suggesting another peak. As in Fig.3 the peaks must cover overlapping distributions to correspond to an almost equilateral triangle. In the case of  $0^+$  a very broad peak appears around 3, and the other two peaks are around 0.8. This gives rise to an obtuse triangle with side ratios 1.7:1:1.

#### IV. SUMMARY AND CONCLUSIONS

We have computed the  $\alpha$ -particle momentum distributions of 14 three-body decaying low-lying  $^{12}\text{C}$  many-body resonances with 10 different angular momenta and parities. The results are exhibited as single  $\alpha$  energy distributions and energy correlations of Dalitz plots. We assume that the decays of the resonances are independent of their formation as for compound nuclear reactions. We use a three- $\alpha$  cluster model to describe all states even at small distances where the cluster model sometimes fails badly and the many-body structure is indispensable for a structure computation. The idea is, the same as for the classical  $\alpha$ -emission, that three  $\alpha$ -particles must be formed at small or intermediate distances as they emerge at large distances after the decay. Thus the small distance properties should only supply boundary conditions and impose energy and angular momentum conservation. This we mock up in the  $3\alpha$  cluster model by a three-body interaction adjusted to reproduce the resonance energy. Again a simple analogy is found in the preformation factors in  $\alpha$ -emission.

An extreme example is the isospin 1 state which cannot be formed by  $\alpha$ -clusters. Its  $\alpha$ -decay width is consequently very small but still the resulting distributions are with the present assumptions predicted to be essentially the same as the  $1^+$  isospin 0 state.

For three-body decays the interest, and the complication, is how the energy is shared between the three particles. This is determined by the “dynamic evolution” of the resonances, i.e. by the change in structure from small to large distances. To a large extent the de-

cisive properties are symmetries from angular momentum and parity conservation. The resulting momentum distributions carry information about both initial resonance state and the intermediate configurations (decay mechanisms). The only energetically allowed two-body structure is the ground state of  $^8\text{Be}$ . Sequential decay through this state is dominating for natural parity states for the lowest resonance of a given angular momentum. The momentum distributions for the fractions decaying directly are predicted for all resonances below the proton separation threshold.

Whenever possible we give a geometric description of the parts decaying directly to the three-body continuum. This is expressed as side ratios of the  $\alpha$ -particles emerging in a triangle.

The Dalitz plots and  $\alpha$ -energy distributions differ from state to state. A complementary observable is the correlation between the direction of one particle and the center of mass of the other two. These distributions could be used to assign spin and parity to these decaying states as soon as sufficiently accurate experimental data become available. The directly measured angular distribution must contain information about the angular momentum of one particle with respect to the center of mass of the other two particles at large distances. Since several partial waves may contribute this information is not unique, and may have to be supplemented with other information. Furthermore, the uncertainty remains of how the measured large-distance properties reflect the small and intermediate-distance structures of the resonance wave function. Only a theoretical model can provide this connection.

In conclusion, we provide systematic and detailed decay information (fraction of sequential decay, Dalitz plots, single- $\alpha$  energy distributions, momentum direction correlations), which can be compared to upcoming experimental data, for each of the 14 lowest  $^{12}\text{C}$  resonances decaying by  $3\alpha$ -emission.

## Acknowledgments

R.A.R. acknowledges support by a post-doctoral fellowship from Ministerio de Educación y Ciencia (Spain).

- 
- [1] H. Morinaga, Phys. Rev. **101**, 254 (1956).
  - [2] N. De Takacsy and S. Das Gupta, Phys. Lett. B **33**, 556 (1970).
  - [3] H. Friedrich, L. Satpathy and A. Weiguny, Phys. Lett. B **36**, 189 (1971).
  - [4] E. Uegaki, S. Okabe, Y. Abe and H. Tanaka. Prog. Theor. Phys. **57**, 1262 (1977).
  - [5] R. Pichler, H. Oberhammer, A. Csóto and S.A. Moszkowski, Nucl. Phys. A **618**, 55 (1997).
  - [6] P. Descouvemont, Nucl. Phys. A **709**, 275 (2002).
  - [7] T. Neff and H. Feldmeier, Nucl. Phys. A **738**, 357 (2004).
  - [8] S.I. Fedotov, O.I. Kartavtsev, V.I. Kochkin and A.V. Mal'kh, Phys. Rev. C **70**, 014006 (2004).
  - [9] C. Kurokawa and K. Katō, Nucl. Phys. A **792**, 87 (2007).
  - [10] M. Freer, Rep. Prog. Phys. **70**, 2149 (2007).
  - [11] B. John, Y. Tokimoto, Y.-W. Lui, H. L. Clark, X. Chen, and D. H. Youngblood, Phys. Rev. C **68**, 014305 (2003).
  - [12] M. Itoh et al., Nucl. Phys. A **738** (2004) 268.
  - [13] C. Aa. Diget et al., Nucl. Phys. A **760** (2005) 3.
  - [14] T. Takahashi, Phys. Rev. C **16**, 529 (1977).
  - [15] D.P. Balamuth *et al.* Phys. Rev. C **10**, 975 (1974).
  - [16] A.A. Korshennikov, Yad. Fiz. **52**, 1304 (1990); Sov. J.

- Nucl. Phys. **52**, 827 (1990).
- [17] R.H. Dalitz, *Phylos. Mag.* **44**, 1068 (1953).
- [18] R. Álvarez-Rodríguez, E. Garrido, A.S. Jensen, D.V. Fedorov and H.O.U. Fynbo, *Eur. Phys. J. A* **31**, 303 (2007).
- [19] Y.K. Ho, *Phys. Rep.* **99**, 1 (2002).
- [20] D.V. Fedorov, E. Garrido, and A.S. Jensen, *Few-body systems*, **33**, 153 (2003).
- [21] E. Nielsen, D.V. Fedorov, A.S. Jensen, and E. Garrido, *Phys. Rep.* **347**, 373 (2001).
- [22] E. Garrido, D.V. Fedorov, A.S. Jensen and H.O.U. Fynbo, *Nucl. Phys. A* **766**, 74 (2005).
- [23] R. Álvarez-Rodríguez, A.S. Jensen, D.V. Fedorov, H.O.U. Fynbo and E. Garrido, *Phys. Rev. Lett.* **99**, 072503 (2007).
- [24] D.V. Fedorov, H.O.U. Fynbo, E. Garrido and A.S. Jensen, *Few-body systems*, **34**, 33 (2004).
- [25] S. Ali and A.R. Bodmer, *Nucl. Phys.* **80**, 99 (1966).
- [26] D. V. Fedorov and A. S. Jensen, *Phys. Lett. B* **389**, 631 (1996).
- [27] I. J. Thompson, B. V. Danilin, V. D. Efros, J. S. Vaagen, J. M. Bang, and M. V. Zhukov, *Phys. Rev. C* **61**, 024318 (2000).
- [28] C. Aa. Diget, Ph.D. thesis, University of Aarhus, 2006.
- [29] H. O. U. Fynbo, Y. Prezado, U. C. Bergmann, M. J. G. Borge, P. Dendooven, W. X. Huang, J. Huikari, H. Jeppesen, P. Jones, B. Jonson, M. Meister, G. Nyman, K. Riisager, O. Tengblad, I. S. Vogelius, Y. Wang, L. Weissman, K. Wilhelmsen Rolander and J. Äystö, *Phys. Rev. Lett.* **91**, 082502 (2003).
- [30] R. Álvarez-Rodríguez, A.S. Jensen, D.V. Fedorov, H.O.U. Fynbo and E. Garrido, To appear in *J. Phys. G: Conference Series*, nucl-th/0710.5829.
- [31] D.P. Balamuth, R.W. Zurmühle and S.L. Tabor, *Phys. Rev. C* **10**, 975 (1974).
- [32] F. Azjenberg-Selove, *Nucl. Phys. A* **506**, 1 (1990).
- [33] R. Álvarez-Rodríguez, E. Garrido, A.S. Jensen, D.V. Fedorov and H.O.U. Fynbo, *J. Phys. G: Nucl. Part. Phys.* **35**, 014010 (2008).
- [34] M. Freer, I. Boztosun, C.A. Bremner, S.P.G. Chappell, R.L. Cowin, G.K. Dillon, B.R. Fulton, B.J. Greenhalgh, T. Munoz-Britton, M.P. Nicoli, W.D.M. Rae, S.M. Singer, N. Sparks, D.L. Watson and D.C. Weissler, *Phys. Rev. C* **76**, 034320 (2007).
- [35] C. Jacquot, Y. Sakamoto, M. Jung and L. Girardin, *Nucl. Phys. A* **201**, 247 (1072).
- [36] B. Antolkovič and J. Hudomalj, *Nucl. Phys. A* **237**, 253 (1975).
- [37] R. Álvarez-Rodríguez, H.O.U. Fynbo, A.S. Jensen and E. Garrido, submitted for publication (2008).
- [38] Y. Kanada-En'yo, *Prog. Theor. Phys.* **117**, 655 (2007).